Electronic Supplementary Information

One-pot Synthesis of Sub-10 nm $LiNbO_3$ Nanocrystals Exhibiting a Tunable Optical Second Harmonic Response

Rana Faryad Ali[†], *Matthew Bilton*[†], *Byron D. Gates*[†,*]

[†] Department of Chemistry and 4D LABS, Simon Fraser University
8888 University Drive Burnaby, BC, V5A 1S6, Canada

* E-mail: bgates@sfu.ca

This work was supported in part by the Natural Sciences and Engineering Research Council (NSERC) of Canada (Grant No. 1077758), and through the Collaborative Health Research Projects (CHRP) Partnership Program supported in part by the Canadian Institutes of Health Research (Grant No. 134742) and the Natural Science Engineering Research Council of Canada (Grant No. CHRP 462260), the Canada Research Chairs Program (B.D. Gates, Grant No. 950-215846) and MNT Financial Assistance (CMC Microsystems, MNT Grant 4279). This work made use of 4D LABS (www.4dlabs.com) and the Center for Soft Materials shared facilities supported by the Canada Foundation for Innovation (CFI), British Columbia Knowledge Development Fund (BCKDF), Western Economic Diversification Canada, and Simon Fraser University. We also thank Dr. Saeid Kamal (4D LABS) for discussions and assistance in acquiring the SHG spectra for the samples.

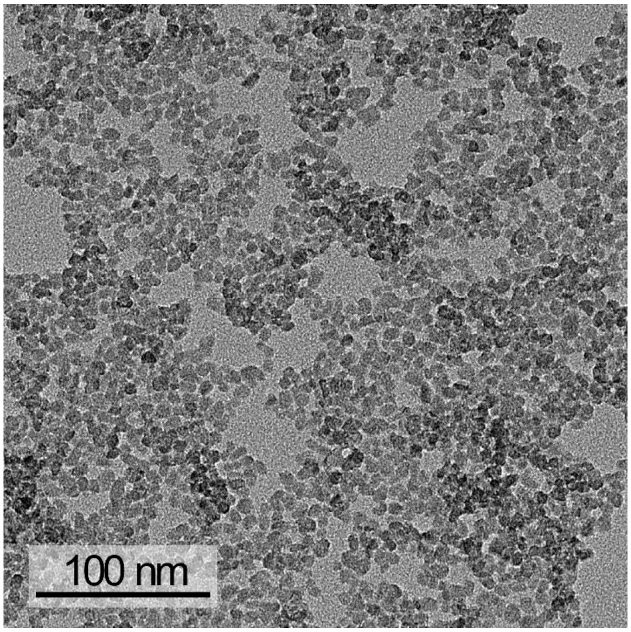

Fig. S1 Transmission electron microscopy (TEM) analysis of lithium niobate ($LiNbO_3$) nanoparticles prepared by the solvothermal reaction.

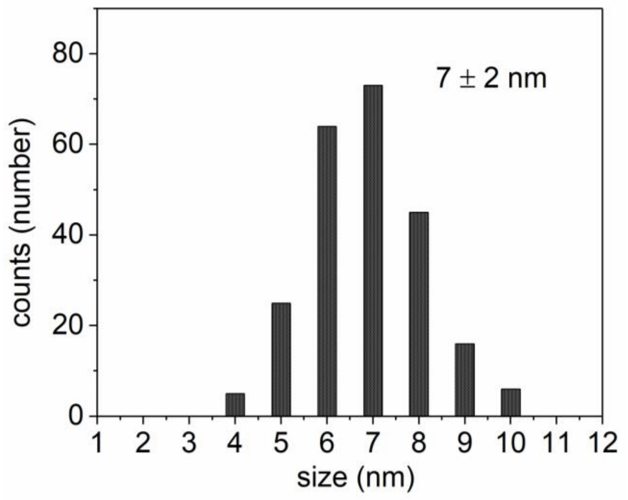

Fig. S2 Histogram depicting the size distribution for the diameters of the $LiNbO_3$ nanoparticles prepared at a reaction time of 96 h. This analysis included measurements obtained from 230 independent nanoparticles. The variance of 2 nm is reported as one standard deviation from the calculated mean of 7 nm.

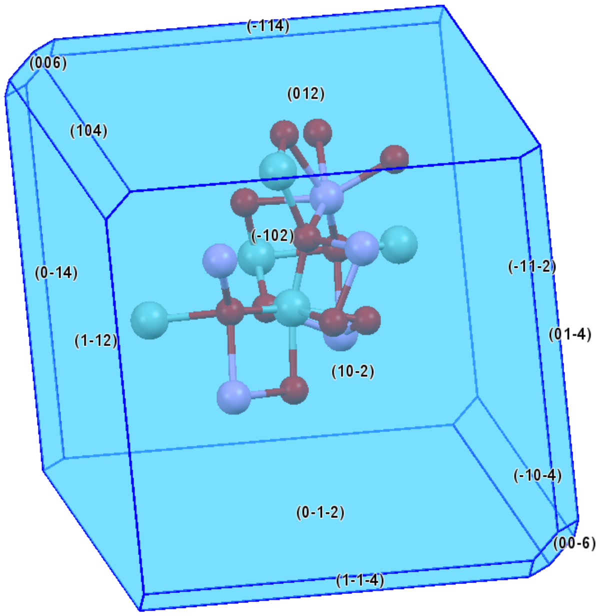

Fig. S3 Bravais-Friedel-Donnay-Harker (BFDH) morphology calculations for $LiNbO_3$ indicated that {012}, {104}, and {006} are dominant facets in a single-crystal product.

Table S1. Ratios between the peak areas as measured from the X-ray diffraction (XRD) reflections for a reported $LiNbO_3$ reference material (JCPDS No. 020-0631) and the nanoparticles of $LiNbO_3$ prepared by the solvothermal synthesis.

XRD peak ratios	reference JCPDS No. 020-0631	96 h product
(104)/(012)	0.37	0.56
(110)/(012)	0.22	0.24
(202)/(012)	0.11	0.75
(116)/(012)	0.25	0.41

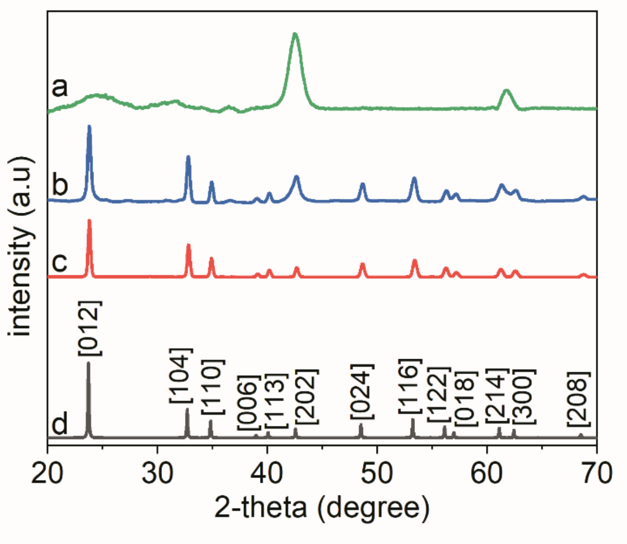

Fig. S4 Powder XRD patterns of the products obtained after reaction times of: (a) 72 h; and (b) 96 h. For comparison, XRD patterns are included for: (c) a commercial $LiNbO_3$ powder purchased from Sigma Aldrich; and (d) a reported $LiNbO_3$ reference material (JCPDS No. 020-0631).

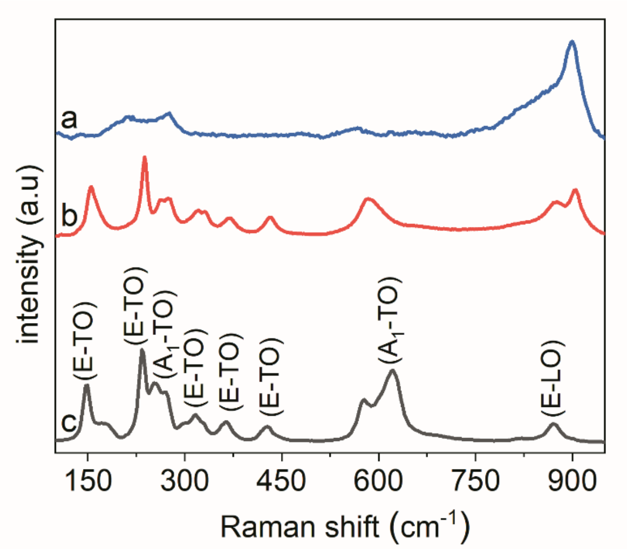

Fig. S5 Raman spectra for the products obtained at reaction times of: (a) 72 h; and (b) 96 h. For comparison, a Raman spectrum is included for (c) a commercial $LiNbO_3$ powder purchased from Sigma Aldrich.

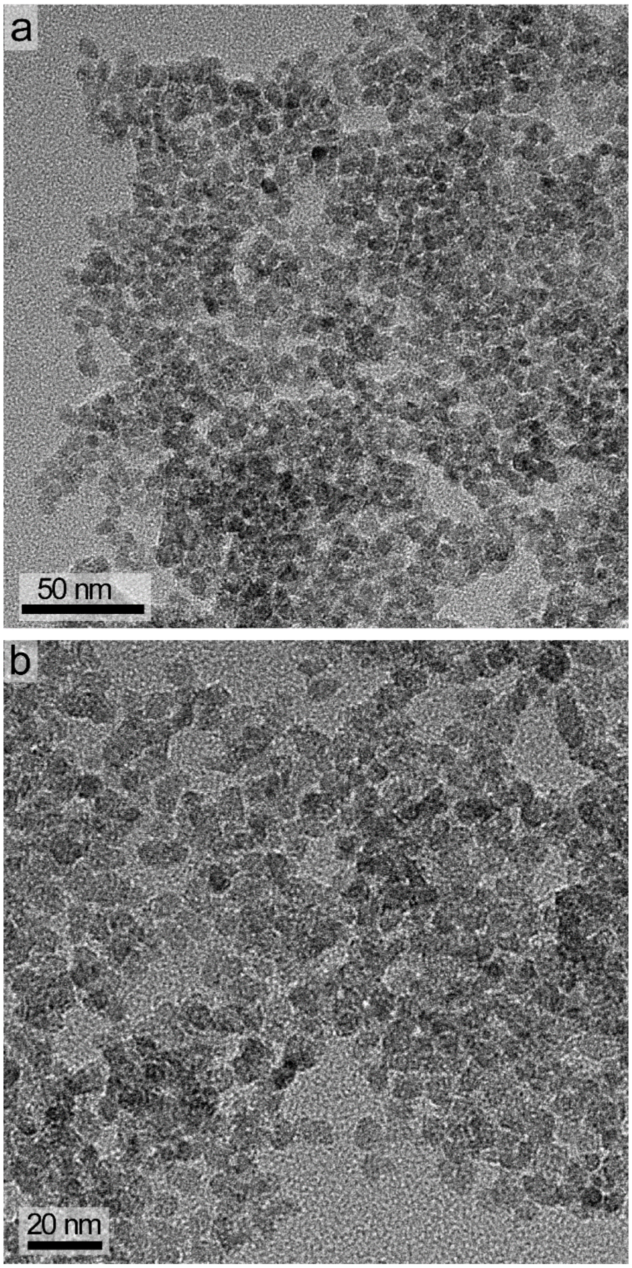

Fig. S6 Representative TEM images of the product obtained after a reaction time of 3 d.

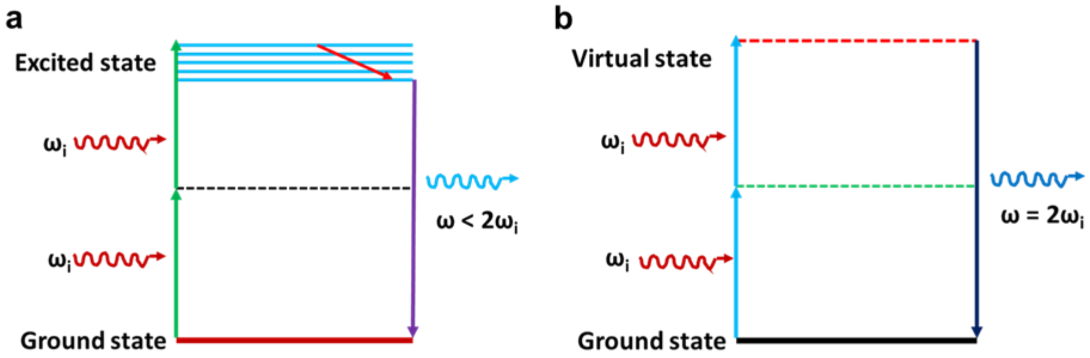

Fig. S7 Schematic diagrams for optical transitions associated with non-linear optical excitation and the corresponding photon emission: (a) a Perrin–Jablonski fluorescence diagram demonstrating that a two-photon induced fluorescence results from the absorption of two photons of an appropriate frequency (ω_i), followed by a vibrational relaxation to the lowest energy level of the excited electronic states. Subsequent relaxation to the ground state results in a spontaneous fluorescence emission of a photon with an energy equivalent to less than $2\omega_i$; and (b) a depiction of second harmonic generation (SHG) in which two incident photons of a frequency (ω_i) are converted into a single photon with double the frequency ($2\omega_i$) of the incident photons. This conversion involves a virtual excited state.

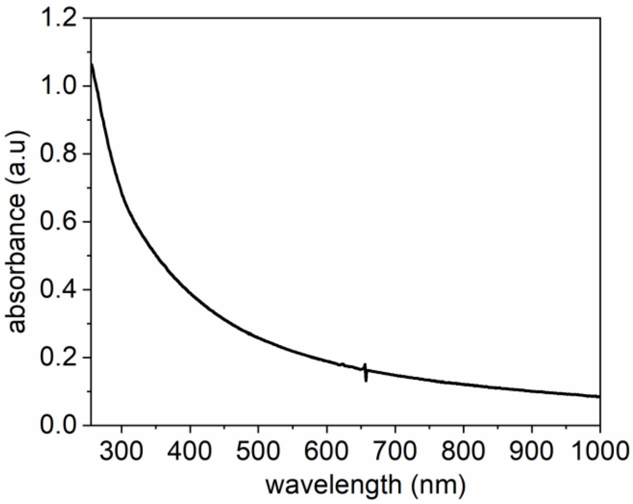

Fig. S8 Ultraviolet (UV)-visible absorption spectrum of a suspension of the ~7-nm diameter $LiNbO_3$ nanocrystals in an ethanol solution. This spectrum indicates the optical transparency of these nanoparticles from ~400 to 1000 nm. The non-linear background is associated with an absorbance edge of the $LiNbO_3$ particles. This contribution can be further observed in the details provided in Fig. S9.

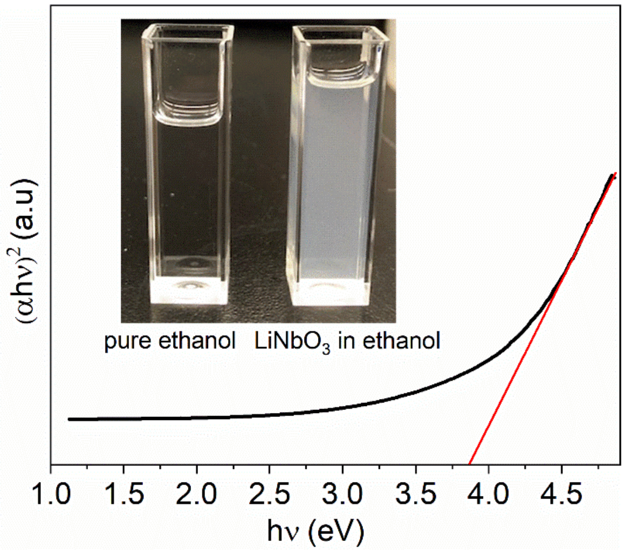

Fig. S9 Analyses of the optical band gap for the LiNbO$_3$ nanoparticles as determined using a Tauc plot. The Tauc plot was obtained by plotting $(\alpha h\nu)^{1/n}$ versus the incident light in values of hν, where α represents the absorption coefficient and n denotes the type of electronic transition involved in the excitation process. A value of n = ½ was used for these analyses, which corresponds to a direct band gap transition. The calculated band gap is 3.85 eV or ~322 nm, which is consistent with prior reports for LiNbO$_3$. [1,2]

The intensity of the SHG signal is dependent on the frequency/wavelength of the fundamental, incident light. This relation is represented in part through Equation S1, listed below.[3,4] This equation shows that an increase in the wavelength of the incident light inversely effects the intensity of the scattered SHG signals. Furthermore, the observed decrease in intensity of the SHG signals also correlates with a decrease in the power of the incident light with an increase in wavelength, which results an increase in the beam waist (Equation S2).[5] It is the combination of these contributions that leads to a decrease in the observed SHG signal with an increase in wavelength of the incident light.

Equation S1 $$I_{2\omega} \propto 16\pi(\omega/n_{\omega}^{2}n_{2\omega}c)^{2}\, kS_{2\omega}^{2}\, |\chi_{eff}^{(2)}|^{2}\, I_{\omega}^{2}$$

Herein,

$I_{2\omega}$, intensity of the SHG signal

ω, frequency of the fundamental excitation

n_{ω}, refractive index of the material at the fundamental wavelength of the excitation

$n_{2\omega}$, refractive index of the material at the second harmonic wavelength

2ω, frequency of the SHG signal

c, speed of light

k, a function related to the particle size

$S_{2\omega}$, backscattering coefficient at 2ω

$\chi_{eff}^{(2)}$, second order susceptibility of the material

I_{ω} , intensity of the fundamental excitation wavelength

Equation S2 $$\omega_0 = \frac{1.27 \times f \times \lambda}{d} \approx \frac{1.27 \times \lambda}{2NA}$$

Herein,

ω_0, beam waist/radius

d, clear aperture

f, focal length

λ, wavelength of incident light

NA, numerical aperture of the lens

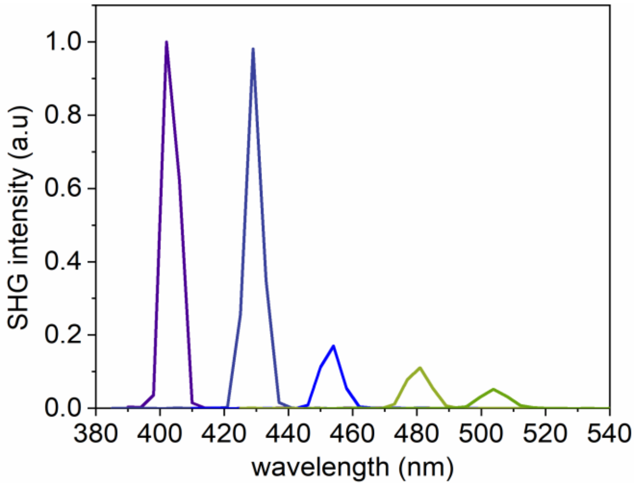

Fig. S10 Relative intensity of the SHG signal obtained from the ~7-nm diameter $LiNbO_3$ nanoparticles as obtained at 400, 425, 450, 475 and 500 nm when excited with incident wavelengths of 800, 850, 900, 950 and 1000 nm, respectively. For comparative purposes, the SHG intensities of were each normalized against the maximum intensity of the SHG signal that was measured at 400 nm when the incident light was 800 nm.

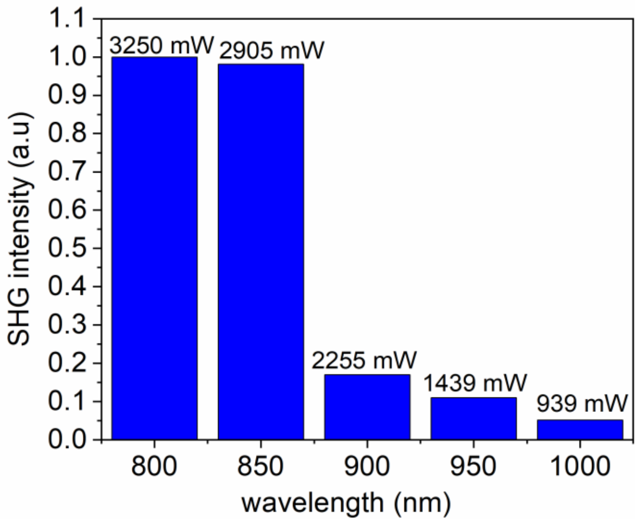

Fig. S11 Dependence of the relative SHG intensity on the wavelength and power of the incident excitation produced by a tunable femtosecond laser. The power of the laser pulses decreased with an increase in the incident wavelength as indicated by the values labelled on the graph. The decreased power of the incident light with increasing wavelength, attributed in part to an increased spread in the spot size of the incident laser beam at the sample for the longer wavelengths (see, for example, Equation S2), resulted in a corresponding decrease in the measured SHG intensity. The power reported for the incident excitation corresponds with the beam power as generated at the laser cavity.

References

[1] J. Castillo-Torres, *Phys. Status Solidi*, 2013, **250**, 1546.

[2] E. Lamouroux, L. Badie, P. Miska and Y. Fort, *Inorg. Chem.*, 2016, **55**, 2246.

[3] Y. Guo, P. P. Ho, H. Savage, D. Harris, P. Sacks, S. Schantz, F. Liu, N. Zhadin and R. R. Alfano, Opt. Lett., 1997, **22**, 1323.

[4] Y. R. Shen, Nature, 1989, **337**, 519.

[5] M. Shen, PhD thesis, The University of British Columbia, 2015.